

Multimodal Medical Image Binding via Shared Text Embeddings

Yunhao Liu*

The Hong Kong Polytechnic University
Hong Kong, China

yunhao.liu@connect.polyu.hk

Suyang Xi*

Emory University
Atlanta, USA

Shiqi Liu*

The University of Hong Kong
Hong Kong, China

Hong Ding

University of Illinois Chicago
Chicago, USA

Chicheng Jin

University of Science and Technology of China
Hefei, China

Chong Zhong

The Hong Kong Polytechnic University
Hong Kong, China

Junjun He

Shanghai AI Laboratory
Shanghai, China

Catherine C. Liu†

The Hong Kong Polytechnic University
Hong Kong, China

catherine.chunling.liu@connect.polyu.hk

Yiqing Shen†

Johns Hopkins University
Baltimore, USA

yiqingshen1@gmail.com^{*†}

Abstract

Medical image analysis increasingly relies on the integration of multiple imaging modalities to capture complementary anatomical and functional information, enabling more accurate diagnosis and treatment planning. Achieving aligned feature representations across these diverse modalities is therefore important for effective multimodal analysis. While contrastive language-image pre-training (CLIP) and its variant have enabled image-text alignments, they require explicitly paired data between arbitrary two modalities, which is difficult to acquire in medical contexts. To address the gap, we present Multimodal Medical Image Binding with Text (M^3Bind), a novel pre-training framework that enables seamless alignment of multiple medical imaging modalities through a shared text representation space without requiring explicit paired data between any two medical image modalities. Specifically, based on the insight that different images can naturally bind with text, M^3Bind first fine-tunes pre-trained CLIP-like image-text models, which are derived from different medical modalities, to align their modality-specific text embedding space while preserving

their original image-text alignments. Subsequently, we distill these modality-specific text encoders into a unified model, creating a shared text embedding space. Notably, M^3Bind is a flexible framework in which the selection of CLIP-like models is not fixed and can be adapted according to the requirements of the task. Experiments on X-ray, CT, retina, ECG, and pathological images on multiple downstream tasks demonstrate that M^3Bind achieves competitive or even superior performance in zero-shot, few-shot classification and cross-modal retrieval tasks compared to its CLIP-like counterparts. These results validate M^3Bind 's effectiveness in achieving cross-image-modal alignment for medical analysis.

1. Introduction

Medical diagnosis is increasingly based on the integration of multiple imaging modalities that provide complementary anatomical and pathological information [18]. For example, computed tomography (CT) enables high resolution 3D tissue visualization [35], chest radiographs offer a broad structural context [40], retina imaging captures microvascular patterns [27], electrocardiogram (ECG) records the electrical activity of the heart [30], and histopathology pro-

*Equal contribution.

†Corresponding author.

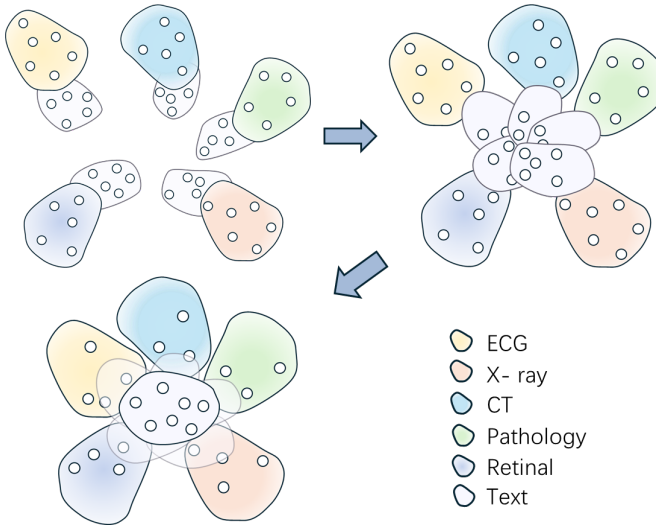


Figure 1. We illustrate the M³Bind framework, designed to embed multiple medical imaging modalities (X-ray, CT, retina, ECG, and Pathology) within a cohesive text-anchored space. In this figure, the transition from Phase One to Phase Two represents the five modality-specific CLIP-like models we used. These models start by aligning each modality with the text modality in isolation and then use text as the anchor modality, achieving joint alignment of all modalities through alignment with different text encoders. The progression from Phase Two to Phase Three indicates the further distillation of knowledge from the five aligned modality-specific text encoders into a unified text encoder, to achieve a consistent representation of all texts paired with different modalities.

vides tissue visualization at the cell level [29]. While each modality contributes unique diagnostic information, their full potential emerges when analyzed together in a multimodal fashion [5]. For example, the evaluation of respiratory diseases benefits from integrating the detailed visualization of the lung parenchyma of CT with the broader anatomical context provided by X-rays [4]. Similarly, cardiovascular diagnostics leverage the synergy between retinal vasculature patterns and histopathological tissue examination to evaluate both structural and functional aspects of cardiac health [33]. Conditions such as pericarditis require the combination of ECG data showing changes in the ST segment and PR segment with chest radiographs that reveal the cardiac silhouette or pericardial calcification [1]. These clinical scenarios highlight the importance of aligned feature representations that can effectively synthesize diagnostic information across diverse medical imaging modalities [11].

Contrastive language image pre-training (CLIP) [34] can align embedding spaces between visual and textual information through contrastive learning [24, 25, 32, 52]. In

medical image analysis, specialized CLIP variants have been proposed to integrate specific medical images with the corresponding clinical text descriptions [56]. For radiology applications, GLORIA [16] and MGCA [46] improve diagnostic interpretability by aligning chest X-rays with radiology reports, while CT-CLIP [13] extends this framework to volumetric CT data analysis. In ophthalmology and pathology domains, FLAIR [38] and QuiltNet [19] respectively leverage semantic supervision for zero-shot retinal diagnosis and fine-grained histological interpretation. However, these approaches typically focus on alignment between a single medical imaging modality and text, limiting their applicability to multiple medical imaging modalities [16, 46]. For n different modalities, conventional CLIP-based approaches would require training $\binom{n}{2} = \frac{n(n-1)}{2}$ separate alignment models, which is not only computationally intensive but also limited by the difficulty of acquiring the corresponding paired data between different imaging types.

Recent work in multimodal learning demonstrates that diverse modalities can be aligned in a shared embedding space without requiring explicit pairwise training. Specifically, ImageBind [10] uses natural images as a bridge to connect six different data modalities through their inherent connections to visual information. However, direct application of ImageBind to medical imaging is not applicable due to the lack of an anchor visual modality. Alternatively, “*binding through images*” concept inspires our approach to multimodal medical imaging, where diverse modalities frequently co-occur with clinical text descriptions that can serve as semantic bridges. For example, radiological images are routinely accompanied by detailed reports, pathology slides with diagnostic annotations, and retina scans with clinical evaluations. This motivates the use of clinical text as a semantic anchor to align diverse medical imaging modalities in a unified representation space (Figure 1).

To bridge the gap, we propose multimodal medical image binding with text (M³Bind), a multimodal pre-training framework for medical image analysis. M³Bind innovates by its fine-tuning of CLIP-like models across multiple modalities, using text as an anchor modality to bind to various medical imaging modalities. Unlike previous CLIP-like methods, M³Bind creates a shared text representation space by aligning the text modalities of all CLIP-like models, thereby aligning different image modalities without requiring explicit paired data between any two image modalities. We further employ distillation [14, 21, 31, 36, 43, 48] to consolidate modality-specific text encoders into a unified model that enables seamless cross-modal analysis.

The main contributions are four-fold. Firstly, we propose M³Bind, a novel multimodal pre-training framework that addresses the challenge of cross-modal medical image alignment by using text as a central bridging modality, enabling seamless and flexible integration of multi-

ple CLIP-like image-text encoders without requiring explicit paired data between image modalities. Secondly, we propose an adaptive training strategy that effectively counters the inherent modality imbalance between different medical image modalities, ensuring balanced representation learning across diverse modalities. Thirdly, we introduce Shared Embedding Space Knowledge Distillation to consolidate representations from multiple modality-specific text encoders into a single unified text model, enhancing computational efficiency while preserving alignment quality across modalities. Finally, we conduct a comprehensive evaluation of M³Bind on 12 diverse datasets that span X-ray, CT, retina, ECG, and pathological images, demonstrating state-of-the-art performance in zero shot classification, few shot classification, and cross-modal retrieval tasks compared to existing CLIP-based approaches.

2. Related Work

2.1. CLIP Variants

CLIP has inspired numerous adaptations that improve multimodal representation learning in diverse domains. Early attempts focused on representation quality, where SLIP [32] incorporated self-supervised learning objectives alongside contrastive training to improve feature robustness, while DeCLIP [39] leveraged multi-dimensional supervision signals to increase data efficiency. Several later approaches have explored masking strategies to optimize the alignment process. For example, MaskCLIP [7] employed masked self-distillation with an exponential moving average (EMA) encoder to strengthen alignment quality and noise resilience, while FLIP [26] and Alpha-CLIP [42] introduced input masking that balances computational efficiency with model depth and performance. Most relevant to our work, ImageBind [10] advanced multimodal integration by unifying six distinct modalities, including images, text, audio, depth, thermal, and IMU data, into an aligned representation space using images as a bridge modality. Although ImageBind demonstrated impressive performance in tasks in the natural domain, its approach cannot be directly applied to medical imaging contexts where no single image modality can serve as a universal anchor.

2.2. Medical CLIP-like Models

Medical imaging has seen adaptation of CLIP to address domain-specific challenges, which leverage contrastive learning to align medical images with clinical text. For volumetric data analysis, CT-CLIP [13] aligns 3D computed tomography scans with radiology reports. Ophthalmology applications benefit from FLAIR [38], which enriches the analysis of retinal images through the supervision of semantic text, substantially improving zero shot diagnostic capabilities. For chest radiography, MGCA [46] proposes

multi-granularity cross-modal contrastive learning to capture hierarchical disease manifestations. In digital pathology, QuiltNet [19] integrates histopathological images with expert knowledge for the interpretation of fine-grained tissue. Despite these advances, each model operates within a single imaging modality, limiting their utility in comprehensive multimodal analysis scenarios. BiomedCLIP[53] and UniMed-CLIP[22] aim to collect more diverse and extensive data to train models. However, these methods employ a single shared visual encoder for images across different modalities. Given the significant heterogeneity among multimodal medical images, this approach inevitably limits the representational capacity of the model. MedBind [9] represents an initial step toward multimodal integration in medicine by introducing a specialized loss function to handle paired X-ray and ECG data. However, MedBind still relies on explicitly curated image-to-image pairings, which are difficult to obtain at scale across diverse medical imaging modalities. This dependency on paired data presents a constraint for broader multimodal medical image analysis. Our proposed M³Bind addresses this limitation by introducing a text-centric binding approach that eliminates the need for direct image-to-image pairings.

2.3. Knowledge Distillation

In single-modality contexts, Knowledge Distillation (KD) achieved notable success by compressing large networks while preserving performance through the transfer of soft probability distributions rather than hard labels[14]. Regarding multimodal fields, recent attempts include Distil-IVLM [47], which introduced cross-modal attention alignment to preserve vision-language interactions between teacher and student models. Additionally, TinyCLIP [49] used affinity mimicking and weight inheritance to optimize vision language embeddings, although its effectiveness remains constrained by architectural similarity requirements. CLIP-KD [50] overcomes this limitation by supporting knowledge transfer between heterogeneous architectures. Further advances have refined the granularity of knowledge transfer in multimodal models. DIME-FM [41] proposed instance-level distillation to capture fine-grained relationships between individual samples, while CLIP-CID [51] extended this approach with cluster-level distillation that preserves semantic relationships between instance groups. In our M³Bind, we leverage KD to address the challenge of unifying multiple modality-specific text encoders into a single model while preserving alignment with diverse medical imaging modalities.

with these modality-specific pre-trained image-text models, each trained on their respective medical imaging modality with corresponding textual descriptions. The selection of these models is flexible and can be freely chosen according to specific needs, not limited to the models we have actually selected. The first stage of M³Bind establishes text as a shared semantic space by aligning the text embedding spaces of these five CLIP-like models while preserving their respective original image-text alignments through contrastive learning. Specifically, for each modality m , we maintain the alignment of image and text using the following contrastive loss:

$$\mathcal{L}_{CLIP}^{(m)} = - \sum_{i=1}^N \log \frac{\exp(\text{sim}(\mathbf{I}_i^{(m)}, \mathbf{T}_i^{(m)}) / \tau)}{\sum_{j=1}^N \exp(\text{sim}(\mathbf{I}_i^{(m)}, \mathbf{T}_j^{(m)}) / \tau)}, \quad (1)$$

where $\mathbf{I}_i^{(m)}$ represents the image embedding of modality m and $\mathbf{T}_i^{(m)}$ denotes the corresponding text embeddings, τ is the temperature scaling factor, and N denotes the batch size of paired image-text samples. To align the text embedding spaces across different modalities, we employ a mean squared error (MSE) loss between arbitrary modality-specific text encoders, namely

$$\mathcal{L}_{MSE}^{(m_1, m_2)} = \frac{1}{N} \sum_{i=1}^N |\mathbf{T}_{m_1, i} - \mathbf{T}_{m_2, i}|^2 \quad (2)$$

where $\mathbf{T}_{m_1, i}$ and $\mathbf{T}_{m_2, i}$ represent text embeddings with respect to different image modalities m_1 and m_2 corresponding to the same semantic content i . By minimizing this distance, we encourage the convergence of diverse modality-specific text representations from different text encoders into an aligned space.

3.3. Adaptive Modality Balancing

Medical datasets with respect to different modalities vary substantially in size, with X-ray collections often containing millions of images, while ECG and retinal images may be orders of magnitude smaller. To address this inherent modality imbalance, M³Bind incorporates an adaptive modality balancing strategy with three components. First, we employ an adaptive sampling approach that dynamically adjusts the probability of selecting text data from each modality during training. For any modality m , the sampling probability is inversely proportional to its dataset size $|D_m|$, namely

$$p_m = \frac{(1/|D_m|)^\beta}{\sum_{m=1}^M (1/|D_m|)^\beta}, \quad (3)$$

where β is the balancing hyperparameter that controls the degree of compensation for underrepresented modalities. Higher values of β increase the sampling frequency of

smaller datasets, while $\beta = 0$ would result in uniform sampling regardless of dataset size. We empirically set $\beta = 0.5$ in our experiments. Second, we implement modality-specific learning rate scaling to optimize convergence across datasets of varying sizes. The learning rate η_m for each modality m is adjusted according to

$$\eta_m = \frac{\eta_0}{\sqrt{|D_m|}}, \quad (4)$$

where η_0 represents the base learning rate. It allows smaller datasets to benefit from more aggressive parameter updates while preventing overfitting on larger datasets through more conservative updates. Third, we incorporate modality-specific loss weighting to ensure balanced optimization across all imaging types. Each modality is assigned a weight inversely proportional to its dataset size, namely

$$w_m = \frac{1}{\sqrt{|D_m|}}. \quad (5)$$

These weights are applied to the total objective function, ensuring that smaller datasets receive appropriate emphasis during training. The complete training objective integrates these balancing mechanisms into:

$$\mathcal{L}_{total} = \sum_{m=1}^M w_m \cdot \mathcal{L}_{CLIP}^{(m)} + \lambda \cdot w_{m_1} \cdot w_{m_2} \cdot \sum_{m_1 \neq m_2} \mathcal{L}_{MSE}^{(m_1, m_2)}. \quad (6)$$

where the first term represents the weighted sum of modality-specific CLIP losses in Eq. (1), maintaining intra-modality alignment, and the second term aggregates MSE losses between all pairs of modalities (m_1, m_2) to enforce alignment between the text embeddings. The hyperparameter λ is the balancing coefficient. To preserve the well-established representational capabilities of the pre-trained CLIP-like models while efficiently adapting them to our multi-modal context, we leverage Low-Rank Adaptation (LoRA) [15] in optimizing Eq. (6).

3.4. Shared Embedding Space Knowledge Distillation

To consolidate the text embedding space into a single unified model, we propose Shared Embedding Space Knowledge Distillation (SESKD). The SESKD employs modality-specific text encoders as teachers, including ones for X-ray, Retina, Pathology, ECG, and CT, and distills their collective knowledge into a single student model based on BioClinicalBERT [2]. We choose BioClinicalBERT as it has been pre-trained specifically on biomedical and clinical text, providing domain-appropriate linguistic representations that align with the medical context of our imaging modalities. Our distillation process operates through two objectives. First, we apply a MSE loss to align the student's text embeddings with each teacher encoder's output,

namely

$$\mathcal{L}_{\text{KD}} = \sum_{m=1}^M \text{MSE}(\mathbf{T}_m, \mathbf{T}_{\text{student}}), \quad (7)$$

where \mathbf{T}_m represents each teacher text encoder’s output embedding, and $\mathbf{T}_{\text{student}}$ is the corresponding embedding from the student model. However, simply matching embeddings is insufficient to preserve the alignment between text and image modalities. Therefore, we incorporate a contrastive learning objective that enforces semantic coherence between the student’s text embeddings and the image embeddings from each modality’s image encoder, namely

$$\mathcal{L}_{\text{Contrastive}} = - \sum_{i=1}^N \log \frac{\exp(\text{sim}(\mathbf{T}_{\text{student}}, \mathbf{I}_i)/\tau)}{\sum_{j=1}^N \exp(\text{sim}(\mathbf{T}_{\text{student}}, \mathbf{I}_j)/\tau)}, \quad (8)$$

where $\text{sim}(\mathbf{T}_{\text{student}}, \mathbf{I}_i)$ denotes the cosine similarity between the student’s text embedding $\mathbf{T}_{\text{student}}$ and the corresponding image embedding \mathbf{I}_i from the respective teacher’s image encoder, with τ serving as a temperature parameter to control the sharpness of the similarity distribution. The complete distillation objective integrates both components, depicted as

$$\mathcal{L}_{\text{SESKD}} = \mathcal{L}_{\text{KD}} + \mathcal{L}_{\text{Contrastive}}, \quad (9)$$

4. Experiments

4.1. Pretrained CLIP-like Models Selected

In our experiments, we select the following pre-trained CLIP-like models to train our M³Bind, namely MGCA [46] (specific to the X-Ray image), QuiltNet [19] (specific to the pathology image), FLAIR [38] (specific to the retina image), and CT-CLIP [13] (specific to CT volumes). Regarding the ECG modality, since currently no related CLIP-like work is available, for subsequent fair comparisons, we follow the definition of the MedBind model [9] and train an ECG-CLIP model ourselves, which is then used for M³Bind training. We will primarily compare our approach with the selected CLIP-like models to demonstrate that our pre-training framework not only enables implicit alignment across different image modalities for these models, but also enhances their original performance.

4.2. Experimental Settings

For all experiments, we maintained consistent preprocessing protocols as specified in the original papers for each modality-specific model (FLAIR, MGCA, CT-CLIP, ECG-CLIP, and QuiltNet) [13, 19, 38, 46]. For the pre-training phase, we employed the AdamW optimizer with a base learning rate of $2e-5$, incorporating warm-up and cosine decay schedules to ensure stable convergence. We configured batch sizes according to the complexity of the model and

hardware constraints, namely 72 for most, with the exception of CT-CLIP [13] which required a reduced batch size of 8 due to its larger memory footprint. Text-modality alignment was performed with a batch size of 64 in all domains, using our adaptive sampling strategy to balance representation in datasets of different sizes. Training was carried out for 15,000 iterations with the balance factor λ set to 10, prioritizing inter-modality text alignment before connecting the individual medical imaging modalities through the unified text space. In the SESKD training, we utilized a pre-trained BioClinicalBERT model [2] as our student text encoder. The training process was divided into two stages: first, we applied the knowledge distillation loss \mathcal{L}_{KD} for 1,200 iterations to establish baseline alignment, then integrated the complete SESKD objective ($\mathcal{L}_{\text{SESKD}}$) for an additional 1,200 iterations to preserve both embedding similarity and contrastive relationships. All other optimization parameters remained consistent with the previous. All experiments were conducted on seven RTX 4090 GPUs, while the SESKD phase requires an additional RTX 4090 GPU.

4.3. Evaluations in Zero-Shot Manner

For the Retina modality: Experiments on retina images were performed following FLAIR’s settings, which involved prompt mappings and disease-specific descriptions to enhance domain knowledge. Validation was performed on MESIDOR and ODIR datasets to test domain shift and novel class generalization. Comparisons were made with FLAIR- π_{naive} , FLAIR- π_{EK} , CLIP, and BiomedCLIP [53]. Our M³Bind achieved ACA scores [55] of 0.564 and 0.543 on MESIDOR (π_{naive} and π_{EK} , respectively) and 0.480 and 0.672 on ODIR200x3, demonstrating superior performance in both metrics.

For the X-Ray modality: MIMIC-CXR pre-trained models were used to predict CheXpert labels, with performance evaluated on the CheXpert 5x200 test set using accuracy, F1 score, and precision metrics. The baseline comparisons shown in Table 1 included ConVIRT [54], GLORIA, MGCA, and PRIOR[3]. Our model achieved the highest scores, with an accuracy of 35.27, an F1-score of 30.71, and a precision of 34.96.

For the ECG modality: Combining the performance in the MIMIC-ECG internal validation dataset and the PTB-XL external validation dataset, we achieve the best performance. In contrast, MedBind_{NM}, which trains directly from randomly initialized networks, results in a performance loss. Even after introducing a loss function to align ECG and X-Ray, MedBind_{BD}’s performance advantages are not significant.

For the Pathology modality: In addition to CLIP, BiomedCLIP, and QuiltNet, we also compared our approach with PLIP [17], another vision-language pre-training model for pathology. Apart from the SkinCancer dataset, we demon-

Table 1. Zero-Shot Performance Comparison Across Four Modalities (Retina, X-Ray, CT, Pathology) Using M³Bind and Baseline Models.

Methods	Retina				Methods	X-Ray			Methods	Retina			
	MESIDOR[6]		ODIR200x3 ^{??}			CheXpert 200x5[20]				MIMIC-ECG[12]		PTB-XL[45]	
	π_{naive}	π_{EK}	π_{naive}	π_{EK}		Accuracy	F1-Score	Precision		R_1	R_{10}	R_1	R_{10}
CLIP[34]	0.237	0.200	0.445	0.480	ConVIRT[54]	21.30	19.03	17.65	–	–	–	–	
BiomedCLIP[53]	0.224	0.207	0.727	0.583	GLORIA[16]	23.20	15.79	44.01	ECG-CLIP	51.7	95.5	2.2	17.5
FLAIR- π_{naive} [38]	0.545	0.442	0.447	0.470	PRIOR[3]	34.15	29.83	34.38	MedBind _{NM} [9]	50.2	93.9	1.9	18.2
FLAIR- π_{EK} [38]	0.495	0.587	0.420	0.667	MGCA[46]	33.45	29.38	34.01	MedBind _{BD} [9]	53.6	94.5	1.6	19.2
M ³ Bind	0.564	0.543	0.480	0.672	M ³ Bind	35.27	30.71	34.96	M ³ Bind	52.4	95.6	2.3	18.3

Methods	Pathology				Methods	CT							
	SkinCancer[23]	Camelyon[44]	SICAPv2[37]	SkinTumor[23]		CT-RATE[13]				RAD-ChestCT[8]			
	Accuracy					AUC	F1	Acc	Prec	AUC	F1	Acc	Prec
CLIP[34]	0.05	0.62	0.39	0.10	CT-Net[8]	0.603	0.631	0.581	0.239	0.544	0.587	0.540	0.285
BiomedCLIP[53]	0.25	0.53	0.46	0.37	CT-CLIP(ZS)[13]	0.731	0.707	0.668	0.323	0.629	0.642	0.595	0.336
PLIP[17]	0.37	0.59	0.45	0.56	CT-CLIP(VF)[13]	0.756	0.738	0.705	0.353	0.650	0.659	0.659	0.349
QuiltNet[19]	0.45	0.65	0.39	0.58	CT-CLIP(CF)[13]	0.756	0.724	0.689	0.339	0.643	0.649	0.607	0.340
M ³ Bind	0.45	0.66	0.40	0.59	M ³ Bind	0.743	0.742	0.711	0.348	0.648	0.662	0.621	0.352

strate performance improvements over QuiltNet on our other datasets, with overall performance exceeding any baseline.

For the CT modality: Internal validation was carried out on CT-RATE and external validation on RAD-ChestCT. Baseline comparisons included CT-Net[8] and three variants of CT-CLIP (ZS, VF, CF). Our model achieved F1 scores of 0.742 in CLIP-RATE and 0.662 on RAD-ChestCT, reflecting high performance in both datasets.

Overall, M³Bind either outperforms or comes close to outperforming in most cases. Even when it does not win, it does not show a noticeable performance loss compared to the pre-trained models we used.

4.4. Evaluations in Few-Shot Manner

In this evaluation, for better comparison, we used different few-shot ratios in various modalities, including 1, 5, 10 for the retina and CT images, 1, 4, 8 for ECG, and 1, 10, 100 for X-ray and pathology images. Our M³Bind demonstrated strong cross-modal adaptability, achieving state-of-the-art performance in most benchmarks, as shown in Table 2. For retinal imaging, M³Bind achieved superior performance in both MESIDOR (61.3% at 5-shot, 62.0% at 10-shot) and ODIR200x3 (80.2% at 1-shot, 89.2% at 10-shot), outperforming BiomedCLIP and FLAIR- π_{EK} . In X-Ray analysis, we attained the highest accuracy on CheXpert across all shots (88.07%/ 88.64%/ 88.98%), surpassing prior specialized models like PRIOR and MGCA. Although the original PRIOR paper mentions that MGCA neglects sentence-level clinical information, which is important for complex downstream tasks like multi-label classification on CheXpert, leading to performance that is not as good as expected, we not only surpass the pre-trained model MGCA we use but also directly exceed PRIOR. This gap is particularly evident in the 1-shot scenario. The model showed particular strength in CT interpretation, achieving 78.77% (1-shot) and 83.20% (5-shot) on CT-RATE, and 75.82% (10-shot) on RAD-ChestCT, outperforming all CT-CLIP variants. Notably, our approach demonstrated excep-

Table 2. Few-Shot classification performance (Accuracy %) comparison of M³Bind across different modalities in terms of accuracy (mean \pm standard deviation) against modality-specific state-of-the-art models on ten datasets spanning five distinct medical imaging modalities. Evaluations are conducted with limited training examples to assess cross-modal transfer capabilities. Red and blue highlighting indicates the best and second-best performance, respectively.

Methods	Retina					
	MESIDOR			ODIR200x3		
	1	5	10	1	5	10
CLIP	0.299 \pm 0.02	0.420 \pm 0.03	0.425 \pm 0.04	0.686 \pm 0.02	0.810 \pm 0.03	0.823 \pm 0.04
BiomedCLIP	0.312 \pm 0.03	0.430 \pm 0.04	0.434 \pm 0.03	0.712 \pm 0.02	0.847 \pm 0.03	0.846 \pm 0.04
ImageNet Init	0.293 \pm 0.02	0.413 \pm 0.03	0.407 \pm 0.05	0.615 \pm 0.02	0.805 \pm 0.03	0.813 \pm 0.04
FLAIR- π_{EK}	0.483 \pm 0.05	0.601 \pm 0.04	0.605 \pm 0.03	0.784 \pm 0.03	0.877 \pm 0.04	0.875 \pm 0.05
OURS	0.467 \pm 0.04	0.613 \pm 0.03	0.642 \pm 0.05	0.802 \pm 0.03	0.890 \pm 0.04	0.903 \pm 0.05
Methods	X-Ray			CheXpert		
	RSNA			10		
	1	10	100	1	10	100
ConVIRT	84.17 \pm 0.77	86.92 \pm 0.13	88.74 \pm 0.36	85.02 \pm 0.28	87.58 \pm 0.53	88.21 \pm 0.46
GLORIA	84.12 \pm 0.47	86.83 \pm 0.53	89.13 \pm 0.12	83.61 \pm 0.52	87.40 \pm 0.39	88.34 \pm 0.12
PRIOR	85.74 \pm 0.36	87.08 \pm 0.19	89.22 \pm 0.16	86.16 \pm 0.64	88.31 \pm 0.20	88.61 \pm 0.29
MGCA	85.80 \pm 0.68	87.66 \pm 0.21	89.30 \pm 0.16	85.63 \pm 0.33	87.65 \pm 0.33	88.30 \pm 1.48
OURS	84.48 \pm 0.12	87.54 \pm 0.24	89.35 \pm 0.43	88.07 \pm 0.52	88.64 \pm 0.27	88.98 \pm 0.39
Methods	ECG			ICBEB[28]		
	PTB-XL[45]			4		
	1	4	8	1	4	8
ECG-CLIP	38.83 \pm 1.42	50.17 \pm 0.73	54.37 \pm 0.80	19.72 \pm 0.26	25.49 \pm 0.48	27.44 \pm 0.27
MedBind _{NM} [9]	39.03 \pm —	49.33 \pm —	54.13 \pm —	19.66 \pm —	25.31 \pm —	27.38 \pm —
MedBind _{BD} [9]	39.80 \pm —	50.40 \pm —	53.43 \pm —	19.97 \pm —	26.04 \pm —	28.08 \pm —
M ³ Bind	39.48 \pm 0.99	50.55 \pm 0.31	54.50 \pm 0.64	20.03 \pm 1.86	25.84 \pm 0.41	27.82 \pm 0.17
Methods	Pathology			SICAPv2		
	Camelyon			10		
	1	10	100	1	10	100
CLIP	80.73 \pm 0.53	81.42 \pm 0.21	82.07 \pm 0.14	52.64 \pm 1.91	62.79 \pm 0.57	65.94 \pm 0.43
PLIP	87.26 \pm 0.61	87.42 \pm 0.23	87.45 \pm 0.19	65.49 \pm 0.95	68.97 \pm 0.63	73.15 \pm 0.71
PLIP(FT)	87.50 \pm 0.35	87.57 \pm 0.18	87.53 \pm 0.07	69.54 \pm 0.47	73.18 \pm 0.61	74.85 \pm 0.53
QuiltNet	87.51 \pm 0.32	87.40 \pm 0.13	87.27 \pm 0.09	69.73 \pm 0.78	74.19 \pm 0.48	75.31 \pm 0.36
OURS	87.65 \pm 0.41	87.88 \pm 0.37	87.63 \pm 0.06	68.91 \pm 1.12	74.56 \pm 0.68	75.54 \pm 0.50
Methods	CT			RAD-ChestCT		
	CT-RATE			5		
	1	5	10	1	5	10
CT-Net	63.12 \pm 0.53	67.56 \pm 0.61	69.75 \pm 0.47	58.79 \pm 0.73	63.86 \pm 0.55	67.65 \pm 0.63
CT-CLIP(ZS)	75.85 \pm 0.68	81.17 \pm 0.79	82.42 \pm 0.57	65.37 \pm 0.81	71.57 \pm 0.42	74.58 \pm 0.59
CT-CLIP(VF)	78.34 \pm 0.40	82.90 \pm 0.51	83.06 \pm 0.73	68.02 \pm 0.67	72.45 \pm 0.72	75.42 \pm 0.53
CT-CLIP(CF)	78.08 \pm 0.65	82.85 \pm 0.58	83.58 \pm 0.79	67.81 \pm 0.51	72.28 \pm 0.43	75.13 \pm 0.77
OURS	78.77 \pm 0.52	83.20 \pm 0.46	83.39 \pm 0.61	68.08 \pm 0.41	72.94 \pm 0.69	75.82 \pm 0.57

tional ECG classification capabilities on PTB-XL (50.55% at 4-shot, 54.50% at 8-shot) and ICBEB (20.03% at 1-shot), exceeding MedBind variants. In pathology images, M³Bind achieved record performance on Camelyon (87.65-87.88%) and competitive results on SICAPv2 (74.56% at 10-shot), highlighting cross-modal robustness. Our method maintained strong scaling capabilities, with performance improvements over baselines in extreme low-shot scenarios (1-10 samples), while showing diminishing returns beyond 100 shots, suggesting effective few-shot knowledge trans-

fer.

Figure 3 illustrates the exceptional few-shot learning efficacy of our methodology across several medical imaging modalities, demonstrating superior performance in handling diverse datasets, including ODIR200x3, CheXpert, SICAPv2, and RAD-ChestCT.

4.5. Evaluations in Cross-Modal Manner

Table 3. Cross-modal retrieval performance (Recall Top@1, 5, 10) comparison of M³Bind against two different variants of MedBind. Red and blue highlighting indicate the best and second-best performance, respectively.

Methods	MIMIC-PAIR		
	Top@1	Top@5	Top@10
MedBind _{NM} [9]	1.36	7.86	15.00
MedBind _{BD} [9]	12.86	30.95	55.43
M ³ Bind	1.82	9.64	17.29

To further evaluate the performance of cross-modal alignment between different image modalities, we conducted a cross-modal retrieval task from X-Ray to ECG modalities on the MIMIC-PAIR dataset. According to the experimental results in Table 3, our framework outperforms MedBind_{NM} in Recall Top@1, Recall Top@5, and Recall Top@10, validating that introducing more modalities and more data indeed enhances cross-modal performance.

Notably, the results for MedBind_{BD} are significantly better than both our method and MedBind_{NM}. This is because MedBind_{BD} uses the MIMIC-PAIR training set during the pre-training phase and introduces a loss function to align the X-ray and ECG modalities. Therefore, MedBind_{BD} does not perform this task in a zero-shot manner, making this comparison unfair, and these results should not be considered. We have also discussed the approach of MedBind_{BD}, noting that as the number of modalities increases, the dataset and computational resource requirements for pairwise alignment between modalities become impractical.

4.6. Ablation Study

Ablation Analysis of X-Ray, ECG, Retina, Pathology, and CT Modalities. We conducted an ablation study to evaluate the contributions of X-ray, ECG, retina, pathology and CT images on the ODIR200x3?? and MIMIC-PAIR datasets, as summarized in Table 4. As the number of modalities involved in training increases, the model’s performance gradually improves, especially when the CT modality, which is highly relevant to chest X-Ray and ECG, is added. The experimental results demonstrate that each additional modality incrementally improves the quality of the shared space representation.

Ablation Study of Adaptive Modality Balancing and Shared Embedding Space Knowledge Distillation Modules.

We conducted an ablation study to investigate the individual contributions of the Adaptive Modality Balancing (AMB) and Shared Embedding Space Knowledge Distillation (SESKD) modules within the M³Bind framework, with performance results shown in Table 5. The results indicate that, in the image-to-text zero-shot classification task, the AMB module can effectively improve model performance, while the effect of SESKD is not significant and may even slightly decrease performance. However, in the cross-modal retrieval task between X-Ray and ECG, both modules are very effective. This shows that the AMB can prevent biased alignment, while SESKD can unify the representation of the shared space.

Table 4. Ablation Study on Individual Contributions of X-Ray, ECG, Retina, Pathology, and CT Modalities: Performance is evaluated on the MIMIC-PAIR datasets.

X-Ray	ECG	Retina	Pathology	CT	MIMIC-PAIR		
					Top@1	Top@5	Top@10
✓	✓				1.25	7.03	15.14
✓	✓	✓			1.19	7.62	14.99
✓	✓	✓	✓		1.48	8.21	15.73
✓	✓	✓	✓	✓	1.82	9.64	17.29

Table 5. Ablation Study of AMB and SESKD Modules: Performance Evaluation on the ODIR200x3 and MIMIC-PAIR Datasets Using the M³Bind Framework.

M ³ Bind	AMB	SESKD	ODIR200x3??		MIMIC-PAIR		
			π_{naive}	π_{EK}	Top@1	Top@5	Top@10
✓			0.452	0.622	1.29	6.85	15.52
✓	✓		0.478	0.659	1.65	8.92	17.01
✓		✓	0.440	0.617	1.40	8.27	15.88
✓	✓	✓	0.472	0.667	1.82	9.64	17.29

5. Conclusion

In this paper, we introduce M³Bind, a novel multimodal pre-training method for aligning medical imaging representation. Using an anchored text modality, M³Bind harmonizes image representations across five CLIP-like medical models, allowing cross-modal alignment without relying on arbitrary paired data between two medical image modalities. Experimental results show that our framework not only achieves implicit alignment across different image modalities, but also brings performance improvements to the original models on image-text tasks. The flexibility of our framework allows it to benefit from stronger CLIP-like models—if we select more powerful base models, our framework can accordingly achieve even better performance, potentially reaching state-of-the-art (SOTA) results.

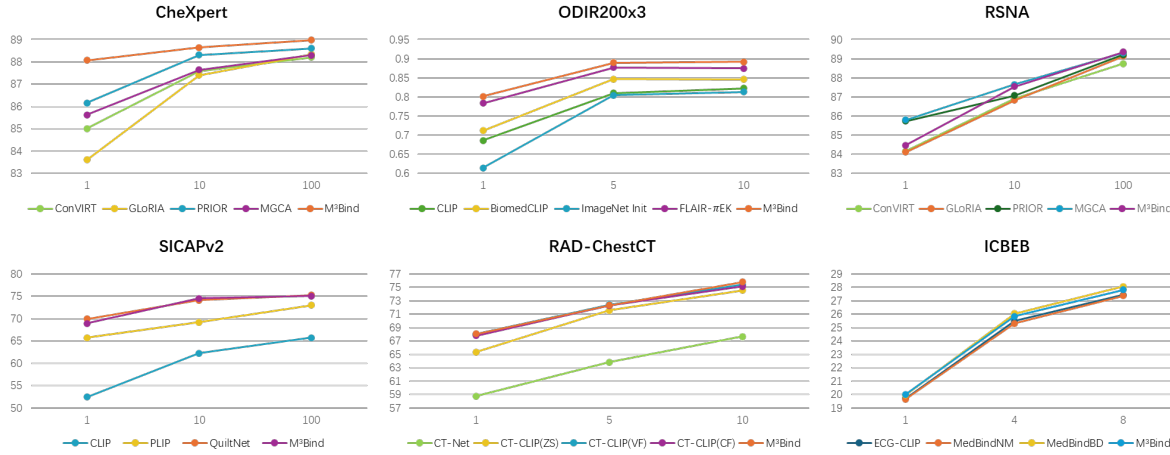


Figure 3. Comparison of Few-Shot Performance Across Various Datasets (ODIR200x3, CheXpert, SICAPv2, RAD-ChestCT) With Increasing Shot Numbers.

References

- [1] Yehuda Adler, Philippe Charron, Massimo Imazio, Luigi Badano, Gonzalo Barón-Esquivias, Jan Bogaert, Antonio Brucato, Pascal Gueret, Karin Klingel, Christos Lionis, Bernhard Maisch, Bongani Mayosi, Alain Pavie, Arsen D Ristić, Manel Sabaté Tenas, Petar Seferovic, Karl Swedberg, Witold Tomkowski, and ESC Scientific Document Group. 2015 esc guidelines for the diagnosis and management of pericardial diseases: The task force for the diagnosis and management of pericardial diseases of the european society of cardiology (esc)endorsed by: The european association for cardio-thoracic surgery (eacts). *European Heart Journal*, 36(42):2921–2964, 2015. 2
- [2] Emily Alsentzer, John R Murphy, Willie Boag, Wei-Hung Weng, Di Jin, Tristan Naumann, and Matthew McDermott. Publicly available clinical bert embeddings. *arXiv preprint arXiv:1904.03323*, 2019. 5, 6
- [3] Pujin Cheng, Li Lin, Junyan Lyu, Yijin Huang, Wenhan Luo, and Xiaoying Tang. Prior: Prototype representation joint learning from medical images and reports. In *Proceedings of the IEEE/CVF International Conference on Computer Vision*, pages 21361–21371, 2023. 6, 7
- [4] Sugama Chicklore, Vicky Goh, Musib Siddique, Arunabha Roy, Paul K Marsden, and Gary JR Cook. Quantifying tumour heterogeneity in 18 f-fdg pet/ct imaging by texture analysis. *European journal of nuclear medicine and molecular imaging*, 40:133–140, 2013. 2
- [5] Fergus Davnall, Connie SP Yip, Gunnar Ljungqvist, Mariyah Selmi, Francesca Ng, Bal Sanghera, Balaji Ganeshan, Kenneth A Miles, Gary J Cook, and Vicky Goh. Assessment of tumor heterogeneity: an emerging imaging tool for clinical practice? *Insights into imaging*, 3:573–589, 2012. 2
- [6] Etienne Decencière, Xiwei Zhang, Guy Cazuguel, Bruno Lay, Béatrice Cochener, Caroline Trone, Philippe Gain, John-Richard Ordóñez-Varela, Pascale Massin, Ali Erginay, et al. Feedback on a publicly distributed image database: the messidor database. *Image Analysis & Stereology*, pages 231–234, 2014. 7
- [7] Xiaoyi Dong, Jianmin Bao, Yinglin Zheng, Ting Zhang, Dongdong Chen, Hao Yang, Ming Zeng, Weiming Zhang, Lu Yuan, Dong Chen, et al. Maskclip: Masked self-distillation advances contrastive language-image pretraining. In *Proceedings of the IEEE/CVF Conference on Computer Vision and Pattern Recognition*, pages 10995–11005, 2023. 3
- [8] Rachel Lea Draelos, David Dov, Maciej A Mazurowski, Joseph Y Lo, Ricardo Henao, Geoffrey D Rubin, and Lawrence Carin. Machine-learning-based multiple abnormality prediction with large-scale chest computed tomography volumes. *Medical image analysis*, 67:101857, 2021. 7
- [9] Yuan Gao, Sangwook Kim, David E Austin, and Chris McIntosh. Medbind: Unifying language and multimodal medical data embeddings. In *International Conference on Medical Image Computing and Computer-Assisted Intervention*, pages 218–228. Springer, 2024. 3, 4, 6, 7, 8
- [10] Rohit Girdhar, Alaaeldin El-Nouby, Zhuang Liu, Mannat Singh, Kalyan Vasudev Alwala, Armand Joulin, and Ishan Misra. Imagebind: One embedding space to bind them all. In *Proceedings of the IEEE/CVF Conference on Computer Vision and Pattern Recognition*, pages 15180–15190, 2023. 2, 3
- [11] Robert Glynne-Jones, Per J Nilsson, Carlo Aschele, Vicky Goh, Didier Peiffert, Andrés Cervantes, and Dirk Arnold. Anal cancer: Esmo–esso–estro clinical practice guidelines for diagnosis, treatment and follow-up. *Radiotherapy and Oncology*, 111(3):330–339, 2014. 2
- [12] Brian Gow, Tom Pollard, Larry A Nathanson, Alistair Johnson, Benjamin Moody, Chrystinne Fernandes, Nathaniel Greenbaum, Jonathan W Waks, Parastou Eslami, Tanner Carbonati, et al. Mimic-iv-ecg: Diagnostic electrocardiogram matched subset. *Type: dataset*, 6:13–14, 2023. 7
- [13] Ibrahim Ethem Hamamci, Sezgin Er, Furkan Almas, Ayse Gulnihan Simsek, Seval Nil Esirgun, Irem Dogan,

- Muhammed Furkan Dasdelen, Bastian Wittmann, Enis Simsar, Mehmet Simsar, et al. A foundation model utilizing chest ct volumes and radiology reports for supervised-level zero-shot detection of abnormalities. *arXiv preprint arXiv:2403.17834*, 2024. 2, 3, 4, 6, 7
- [14] Geoffrey Hinton. Distilling the knowledge in a neural network. *arXiv preprint arXiv:1503.02531*, 2015. 2, 3
- [15] Edward J Hu, Yelong Shen, Phillip Wallis, Zeyuan Allen-Zhu, Yanzhi Li, Shean Wang, Lu Wang, and Weizhu Chen. Lora: Low-rank adaptation of large language models. *arXiv preprint arXiv:2106.09685*, 2021. 5
- [16] Shih-Cheng Huang, Liye Shen, Matthew P Lungren, and Serena Yeung. Gloria: A multimodal global-local representation learning framework for label-efficient medical image recognition. In *Proceedings of the IEEE/CVF International Conference on Computer Vision*, pages 3942–3951, 2021. 2, 7
- [17] Zhi Huang, Federico Bianchi, Mert Yuksekgonul, Thomas J Montine, and James Zou. A visual–language foundation model for pathology image analysis using medical twitter. *Nature medicine*, 29(9):2307–2316, 2023. 6, 7
- [18] Shah Hussain, Iqra Mubeen, Niamat Ullah, Syed Shahab Ud Din Shah, Bakhtawar Abduljalil Khan, Muhammad Zahoor, Riaz Ullah, Farhat Ali Khan, and Mujeeb A Sultan. Modern diagnostic imaging technique applications and risk factors in the medical field: a review. *BioMed research international*, 2022(1):5164970, 2022. 1
- [19] Wisdom Oluchi Ikezogwo, Mehmet Saygin Seyfioglu, Fatemeh Ghezloo, Dylan Stefan Chan Geva, Fatwir Sheikh Mohammed, Pavan Kumar Anand, Ranjay Krishna, and Linda Shapiro. Quilt-1m: One million image-text pairs for histopathology, 2023. 2, 3, 4, 6, 7
- [20] Jeremy Irvin, Pranav Rajpurkar, Michael Ko, Yifan Yu, Silvana Ciurea-Ilcus, Chris Chute, Henrik Marklund, Behzad Haghighi, Robyn Ball, Katie Shpanskaya, et al. Chexpert: A large chest radiograph dataset with uncertainty labels and expert comparison. In *Proceedings of the AAAI conference on artificial intelligence*, pages 590–597, 2019. 7
- [21] Xiaoqi Jiao, Yichun Yin, Lifeng Shang, Xin Jiang, Xiao Chen, Linlin Li, Fang Wang, and Qun Liu. Tinybert: Distilling bert for natural language understanding. *arXiv preprint arXiv:1909.10351*, 2019. 2
- [22] Muhammad Uzair Khattak, Shahina Kunhimon, Muzammal Naseer, Salman Khan, and Fahad Shahbaz Khan. Unimed-clip: Towards a unified image-text pretraining paradigm for diverse medical imaging modalities. *arXiv preprint arXiv:2412.10372*, 2024. 3
- [23] Katharina Kriegsmann, Frithjof Loders, Christiane Zgorzelski, Joerg Kriegsmann, Charlotte Janssen, Rolf Rüdinger MeliB, Thomas Muley, Ulrich Sack, Georg Steinbuss, and Mark Kriegsmann. Deep learning for the detection of anatomical tissue structures and neoplasms of the skin on scanned histopathological tissue sections. *Frontiers in Oncology*, 12:1022967, 2022. 7
- [24] Junnan Li, Dongxu Li, Caiming Xiong, and Steven Hoi. Blip: Bootstrapping language-image pre-training for unified vision-language understanding and generation. In *International conference on machine learning*, pages 12888–12900. PMLR, 2022. 2
- [25] Liunian Harold Li, Pengchuan Zhang, Haotian Zhang, Jianwei Yang, Chunyuan Li, Yiwu Zhong, Lijuan Wang, Lu Yuan, Lei Zhang, Jenq-Neng Hwang, et al. Grounded language-image pre-training. In *Proceedings of the IEEE/CVF Conference on Computer Vision and Pattern Recognition*, pages 10965–10975, 2022. 2
- [26] Yanghao Li, Haoqi Fan, Ronghang Hu, Christoph Feichtenhofer, and Kaiming He. Scaling language-image pre-training via masking. In *Proceedings of the IEEE/CVF Conference on Computer Vision and Pattern Recognition*, pages 23390–23400, 2023. 3
- [27] Gerald Liew, Jie Jin Wang, Paul Mitchell, and Tien Y Wong. Retinal vascular imaging: a new tool in microvascular disease research. *Circulation: Cardiovascular Imaging*, 1(2): 156–161, 2008. 1
- [28] Feifei Liu, Chengyu Liu, Lina Zhao, Xiangyu Zhang, Xiaoling Wu, Xiaoyan Xu, Yulin Liu, Caiyun Ma, Shoushui Wei, Zhiqiang He, Jianqing Li, and Eddie Ng Yin Kwee. An Open Access Database for Evaluating the Algorithms of Electrocardiogram Rhythm and Morphology Abnormality Detection. *Journal of Medical Imaging and Health Informatics*, 8(7):1368–1373, 2018. 7
- [29] Guido Majno and Isabelle Joris. *Cells, tissues, and disease: principles of general pathology*. Oxford University Press, 2004. 2
- [30] David M Mirvis and Ary L Goldberger. Electrocardiography. *Heart disease*, 1:82–128, 2001. 1
- [31] Seyed Iman Mirzadeh, Mehrdad Farajtabar, Ang Li, Nir Levine, Akihiro Matsukawa, and Hassan Ghasemzadeh. Improved knowledge distillation via teacher assistant. In *Proceedings of the AAAI conference on artificial intelligence*, pages 5191–5198, 2020. 2
- [32] Norman Mu, Alexander Kirillov, David Wagner, and Saining Xie. Slip: Self-supervision meets language-image pre-training. In *European conference on computer vision*, pages 529–544. Springer, 2022. 2, 3
- [33] James PB O’connor, Eric O Aboagye, Judith E Adams, Hugo JWL Aerts, Sally F Barrington, Ambros J Beer, Ronald Boellaard, Sarah E Bohndiek, Michael Brady, Gina Brown, et al. Imaging biomarker roadmap for cancer studies. *Nature reviews Clinical oncology*, 14(3):169–186, 2017. 2
- [34] Alec Radford, Jong Wook Kim, Chris Hallacy, Aditya Ramesh, Gabriel Goh, Sandhini Agarwal, Girish Sastry, Amanda Askell, Pamela Mishkin, Jack Clark, et al. Learning transferable visual models from natural language supervision. In *International conference on machine learning*, pages 8748–8763. PMLR, 2021. 2, 7
- [35] Geoffrey D Rubin. Computed tomography: revolutionizing the practice of medicine for 40 years. *Radiology*, 273(2S): S45–S74, 2014. 1
- [36] V Sanh. Distilbert, a distilled version of bert: smaller, faster, cheaper and lighter. *arXiv preprint arXiv:1910.01108*, 2019. 2
- [37] Julio Silva-Rodríguez, Adrián Colomer, María A Sales, Rafael Molina, and Valery Naranjo. Going deeper through

- the gleason scoring scale: An automatic end-to-end system for histology prostate grading and cribriform pattern detection. *Computer methods and programs in biomedicine*, 195: 105637, 2020. 7
- [38] Julio Silva-Rodriguez, Hadi Chakor, Riadh Kobbi, Jose Dolz, and Ismail Ben Ayed. A foundation language-image model of the retina (flair): Encoding expert knowledge in text supervision. *Medical Image Analysis*, 99:103357, 2025. 2, 3, 4, 6, 7
- [39] Stefan Smeu, Elisabeta Oneata, and Dan Oneata. De-clip: Decoding clip representations for deepfake localization. *arXiv preprint arXiv:2409.08849*, 2024. 3
- [40] Anouk M Speets, Yolanda van der Graaf, Arno W Hoes, Sandra Kalmijn, Alfred PE Sachs, Matthieu JCM Rutten, Jan Willem C Gratama, Alexander D Montauban van Swijndregt, and Willem PTHM Mali. Chest radiography in general practice: indications, diagnostic yield and consequences for patient management. *British Journal of General Practice*, 56 (529):574–578, 2006. 1
- [41] Ximeng Sun, Pengchuan Zhang, Peizhao Zhang, Hardik Shah, Kate Saenko, and Xide Xia. Dime-fm: Distilling multimodal and efficient foundation models. In *Proceedings of the IEEE/CVF International Conference on Computer Vision*, pages 15521–15533, 2023. 3
- [42] Zeyi Sun, Ye Fang, Tong Wu, Pan Zhang, Yuhang Zang, Shu Kong, Yuanjun Xiong, Dahua Lin, and Jiaqi Wang. Alpha-clip: A clip model focusing on wherever you want. In *Proceedings of the IEEE/CVF Conference on Computer Vision and Pattern Recognition*, pages 13019–13029, 2024. 3
- [43] Hugo Touvron, Matthieu Cord, Matthijs Douze, Francisco Massa, Alexandre Sablayrolles, and Hervé Jégou. Training data-efficient image transformers & distillation through attention. In *International conference on machine learning*, pages 10347–10357. PMLR, 2021. 2
- [44] Bastiaan S Veeling, Jasper Linmans, Jim Winkens, Taco Cohen, and Max Welling. Rotation equivariant cnns for digital pathology. In *Medical Image Computing and Computer Assisted Intervention—MICCAI 2018: 21st International Conference, Granada, Spain, September 16-20, 2018, Proceedings, Part II 11*, pages 210–218. Springer, 2018. 7
- [45] Patrick Wagner, Nils Strodthoff, Ralf-Dieter Boussejot, Dieter Kreiseler, Fatima I Lunze, Wojciech Samek, and Tobias Schaeffter. Ptb-xl, a large publicly available electrocardiography dataset. *Scientific data*, 7(1):1–15, 2020. 7
- [46] Fuying Wang, Yuyin Zhou, Shujun Wang, Varut Vardhanabhuti, and Lequan Yu. Multi-granularity cross-modal alignment for generalized medical visual representation learning. *Advances in Neural Information Processing Systems*, 35:33536–33549, 2022. 2, 3, 4, 6, 7
- [47] Ning Wang, Jiangrong Xie, Hang Luo, Qinglin Cheng, Jihao Wu, Mingbo Jia, and Linlin Li. Efficient image captioning for edge devices. In *Proceedings of the AAAI Conference on Artificial Intelligence*, pages 2608–2616, 2023. 3
- [48] Kan Wu, Jinnian Zhang, Houwen Peng, Mengchen Liu, Bin Xiao, Jianlong Fu, and Lu Yuan. Tinyvit: Fast pretraining distillation for small vision transformers. In *European conference on computer vision*, pages 68–85. Springer, 2022. 2
- [49] Kan Wu, Houwen Peng, Zhenghong Zhou, Bin Xiao, Mengchen Liu, Lu Yuan, Hong Xuan, Michael Valenzuela, Xi Stephen Chen, Xinggao Wang, et al. Tinyclip: Clip distillation via affinity mimicking and weight inheritance. In *Proceedings of the IEEE/CVF International Conference on Computer Vision*, pages 21970–21980, 2023. 3
- [50] Chuanguang Yang, Zhulin An, Libo Huang, Junyu Bi, Xinqiang Yu, Han Yang, Boyu Diao, and Yongjun Xu. Clip-kd: An empirical study of clip model distillation. In *Proceedings of the IEEE/CVF Conference on Computer Vision and Pattern Recognition*, pages 15952–15962, 2024. 3
- [51] Kaicheng Yang, Tiancheng Gu, Xiang An, Haiqiang Jiang, Xiangzi Dai, Ziyong Feng, Weidong Cai, and Jiankang Deng. Clip-cid: Efficient clip distillation via cluster-instance discrimination. *arXiv preprint arXiv:2408.09441*, 2024. 3
- [52] Lewei Yao, Runhui Huang, Lu Hou, Guansong Lu, Minzhe Niu, Hang Xu, Xiaodan Liang, Zhenguo Li, Xin Jiang, and Chunjing Xu. Filip: Fine-grained interactive language-image pre-training. *arXiv preprint arXiv:2111.07783*, 2021. 2
- [53] Sheng Zhang, Yanbo Xu, Naoto Usuyama, Hanwen Xu, Jaspreet Bagga, Robert Tinn, Sam Preston, Rajesh Rao, Mu Wei, Naveen Valluri, et al. Biomedclip: a multimodal biomedical foundation model pretrained from fifteen million scientific image-text pairs. *arXiv preprint arXiv:2303.00915*, 2023. 3, 6, 7
- [54] Yuhao Zhang, Hang Jiang, Yasuhide Miura, Christopher D Manning, and Curtis P Langlotz. Contrastive learning of medical visual representations from paired images and text. In *Machine Learning for Healthcare Conference*, pages 2–25. PMLR, 2022. 6, 7
- [55] Ziyuan Zhao, Kerui Zhang, Xuejie Hao, Jing Tian, Matthew Chin Heng Chua, Li Chen, and Xin Xu. Bira-net: Bilinear attention net for diabetic retinopathy grading. In *2019 IEEE International Conference on Image Processing (ICIP)*, pages 1385–1389. IEEE, 2019. 6
- [56] Zihao Zhao, Yuxiao Liu, Han Wu, Yonghao Li, Sheng Wang, Lin Teng, Disheng Liu, Zhiming Cui, Qian Wang, and Dinggang Shen. Clip in medical imaging: A comprehensive survey. *arXiv preprint arXiv:2312.07353*, 2023. 2